Tailored Ultrastable Core-shell Au@Ag Nanoparticles for Enhanced Colorimetric Detection in Lateral Flow Assays

Bryan Gosselin,[&,§] *Gilles Bruylants*[&,*] *and Ivan Jabin*[§,*]

[&] Engineering of Molecular NanoSystems, Ecole Polytechnique de Bruxelles, Université libre de Bruxelles (ULB), avenue F. D. Roosevelt 50, CP165/64, B-1050 Brussels, Belgium.

[§] Laboratoire de Chimie Organique, Université libre de Bruxelles (ULB), avenue F. D. Roosevelt 50, CP160/06, B-1050 Brussels, Belgium.

*Corresponding authors: Gilles.Bruylants@ulb.be; Ivan.Jabin@ulb.be

KEYWORDS: Nanomaterials – Core-Shell Nanoparticles – Silver – Lateral Flow Assays – Calix[4]arenes – Troponin

TOC

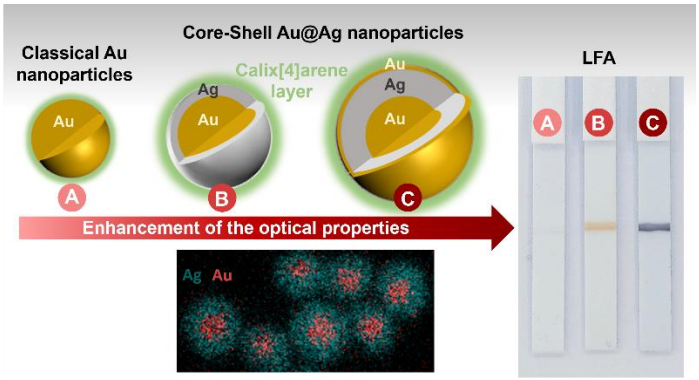

Abstract

In the quest for more effective colorimetric reporters compared to traditional gold nanoparticles, a family of Au@Ag core-shell nanoparticles was designed and synthesized using a seed growth-mediated approach starting from commercial 37 nm AuNPs. This method enabled precise control over the thickness of the silver shell by employing hydroquinone for the reduction of silver and citrate for the stabilization of the resulting core-shell particles. Core-shell NPs with an Ag shell of 7 nm (Au@Ag^{5}NPs) and 18 nm (Au@Ag^{10}NPs) were synthesized resulting in orange and milky yellow suspension, respectively. Additionally, the impact of an external gold layer on Au@Ag^{10}NPs (Au@Ag^{10}@AuNPs), which significantly altered their optical

properties from milky yellow to grey, was investigated. The core-shell Au@AgNPs exhibited substantially higher molar extinction coefficients than their parent AuNPs: from 3.5-fold for Au@Ag^{5}NPs and 9-fold for Au@Ag^{10}NPs and Au@Ag^{10}@AuNPs. Subsequently, all core-shell NPs were functionalized with a calix[4]arene layer, imparting superior stability against external stresses, such as dispersion in PBS, when compared to NPs functionalized with traditional ligands. This calixarene coating enabled the covalent bioconjugation of antibodies on all NP types without inducing noticeable aggregation. Their performance as colorimetric reporters was evaluated in a lateral flow assay for Troponin I detection, demonstrating positive signals down to 1 ng/ml, surpassing the detection limit of the parent gold NPs (2.5 ng/ml). Notably, the grey color of the core-shell Au@Ag^{10}@AuNPs provided strong contrast against the white NC membrane, facilitating T line visualization even at low signal intensity. Despite the lack of optimization of our LFA, it competes with the limit of quantification of commercial LFAs for Troponin I detection, offering the potential for the development of a highly sensitive assay. The diverse core-shell NPs employed in this study form a library of colorimetric reporters with distinct optical properties, paving the way for multiplexed detection systems targeting multiple proteins simultaneously and enhancing diagnostic reliability. Furthermore, the choice of colorimetric reporters allows tailoring the detection range based on the pertinent Limit of Quantification desired for the analyte, dictated by the reporter's light extinction properties.

Introduction

Nanomaterials are extensively studied for their exceptional properties across various fields, including optics, biomedicine, and catalysis.[1–3] In particular, metallic plasmonic nanoparticles, specifically gold (AuNPs) and silver nanoparticles (AgNPs), are known for their superior optical properties compared to conventional organic dyes.[4] These nanoparticles exhibit an extinction band due to the well-known Localized Surface Plasmon Resonance (LSPR). This phenomenon arises from the collective oscillation of free electrons upon light irradiation. When the oscillation frequency of these electrons is in resonance with that of the electric field of light, the plasmonic nanoparticles strongly extinct light.[5] AuNPs are probably the most popular plasmonic nanoparticles in biomedical applications as they are easily synthesized, stable, conjugable with biomolecules and generally considered as biocompatible.[6] In particular, they are extensively used as colorimetric reporters in lateral flow assays (LFA), such as the pregnancy test or the covid antigen test. Typically, AuNPs with a size ranging from 20-40 nm are employed in LFAs. However, their molar extinction coefficient is far from optimal (10^{8}-10^{9}

$M^{-1}cm^{-1}$) and it could be enhanced by both increasing its value or shifting its maximum absorption wavelength to increase the contrast with the NC membrane. For instance, AuNPs with a diameter of 100 nm exhibit a 10^{11} $M^{-1}cm^{-1}$ extinction coefficient.[7] Therefore, recent research efforts have been devoted to the design of plasmonic nanoparticles with higher molar extinction coefficients.[8–10] According to Mie theory, this coefficient depends on the composition, size, external environment, but also on the shape of the nanoparticles.[11] The extinction cross section (σ_{ext}) for spherical particles can be calculated using the following equation (Equation 1):

$$\sigma_{Extinction} = \frac{24\pi^2 R^3 {\varepsilon_m}^{3/2}}{\lambda}\left[\frac{\varepsilon_i}{(\varepsilon_r+2\varepsilon_m)^2+{\varepsilon_i}^2}\right] \qquad \text{Equation 1}$$

where R is the radius of the particles, λ the excitation wavelength, ε_r and ε_i are the real and imaginary parts of the metal's dielectric function, and ε_m the relative dielectric constant of the surrounding medium.

Equation 1 shows that the interaction between a metallic nanoparticle and light strongly depends on the intrinsic dielectric properties of the nanoparticle. Increasing the NPs' diameter results in a cubic rise in σ_{ext}, substantially enhancing their optical characteristics. However, in practice, this strategy is rather limited because nanoparticle size must be inferior to 100 nm for most applications to mitigate issues such as settling or aggregation. For instance, Li *et al.* reported that AuNPs larger than 100 nm are unsuitable for LFA, as gravity dominates their behavior, leading to reduced sensitivity.[8,12] Strategy based on low-density material cores, such as silica, embedded in a metallic shell, allows to overcome this size limitation.[13,14] An alternative approach consists in the modification of the composition of the nanoparticles. Notably, silver nanoparticles possess superior intrinsic optical properties owing to their low ε_i (see Equation 1).[15] Specifically, AgNPs exhibit an LSPR band in the visible region, with a molar extinction coefficient up to one order of magnitude higher than AuNPs of similar size.[4] Despite this advantage, their application in biomedical contexts has been limited.[16] This limitation largely stems from the weak chemical and colloidal stabilities of AgNPs over time or in complex environments. Unlike AuNPs, AgNPs are highly prone to oxidation, making their conjugation with biomolecules difficult to achieve without important particle loss or degradation.[17] Our research group recently demonstrated that the reductive grafting of calix[4]arene tetra-diazonium salts can significantly enhance the stability of both silver nanospheres and nanoplates.[18,19] These preorganized macrocyclic platforms can be strongly

anchored onto surfaces by reducing their four diazonium groups into highly reactive radicals, forming ultra-stable and densely packed thin layers of calix[4]arenes.[20–22] Additionally, the subsequent covalent attachment of biomolecules (e.g. proteins) onto the calix[4]arene-based layer can be easily achieved through classical bioconjugation reactions with the appending functional arms present on the small rim of the calix[4]arenes.[23,24] Furthermore, developing colorimetric reporters with distinct colors is of great interest for multiplex detection. Most of the currently reported multiplex LFAs feature multiple lines of the same color, which may potentially lead to a misinterpretation of the results. Employing lines of distinct colors could circumvent this issue, as each color would correspond to a specific analyte within a single strip.[8] With the aim of developing more efficient colorimetric reporters for LFAs, we envisioned to enhance the molar extinction coefficient of nanoparticles by tuning their size and composition. To achieve this, we decided to develop Au@Ag core-shell nanoparticles. So far, only a few examples of core-shell nanostructures have been reported for SERS-based and colorimetric detection.[25–29] Herein, we describe a synthesis method that enables precise control over the silver shell thickness on a gold core, ensuring high size monodispersity. The stability and bioconjugability of these core-shell nanoparticles were ensured by the grafting of a calix[4]arene layer. This strategy capitalizes on the superior extinction efficiency of the silver shell, while the presence of the gold core alters the UV-Vis spectrum, resulting in a suspension color distinct from that of pure silver nanoparticles. This attribute is particularly relevant for LFA applications, as the yellow color of AgNP suspensions provides a low contrast with the white nitrocellulose membrane. The promising applicability of this new type of nanoparticles as colorimetric reporters in lateral flow assays was subsequently demonstrated through the detection of Troponin I. Detecting minute amounts of this protein is of paramount importance in diagnostics, considering its role as a cardiac biomarker. The presence of Troponin I in blood aids in identifying potential cardiovascular diseases.

Results and discussion

Synthesis of core-shell nanoparticles. Various designs of Au@Ag core-shell nanostructures were developed based on their potential optical advantages (*i.e.* suspension color and/or high molar extinction coefficient). The growth of the silver shell followed a seed-mediated growth procedure, which is known to efficiently control the size and shape of nanoparticles.[30] The thickness of the shell was controlled by adjusting the quantity of silver salt and the number of cycles of addition of the silver salt and reducing agent. In summary, commercially available

citrate-stabilized gold nanoparticles (AuNPs-citrate), with an average size of 37 ± 3 nm, were diluted to an absorbance of 1.5. Then, citrate, hydroquinone and silver nitrate were sequentially added into the suspension at room temperature (Scheme 1). This sequence was repeated either five or ten times with a delay of 2 min between successive addition cycles, resulting in Au@Ag^5 and Au@Ag^{10} NPs-citrate, respectively. The role of hydroquinone was to reduce the silver ions on the gold surface, while citrate acted as a stabilizing agent. Notably, citrate alone was incapable of reducing the silver salt at room temperature, while its absence led to substantial nanoparticle aggregation during the synthesis process (Figure S1).

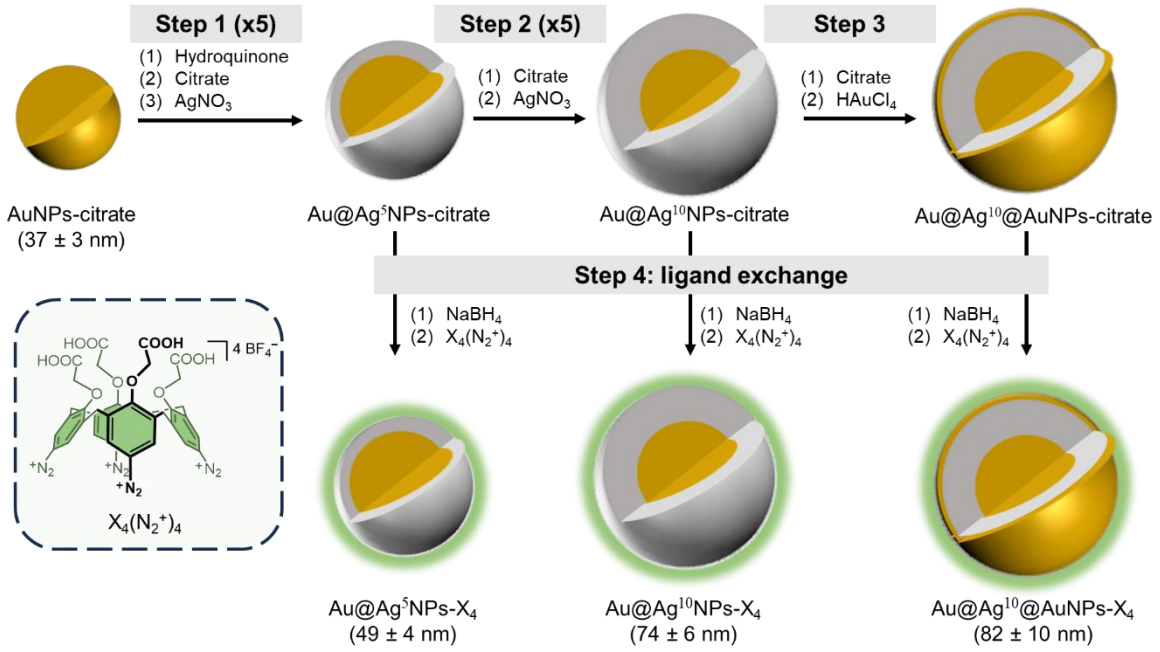

Scheme 1. Synthesis of calix[4]arene-coated core-shell nanoparticles. Inset: structure of calix[4]arene tetra-diazonium salt $X_4(N_2^+)_4$.

UV-Vis spectra of the resulting Au@AgNPs-citrate were recorded after each cycle of additions (Figure 1A). Initially, a small absorbance peak at 520 nm, related to the gold core, was observed. Subsequently, a second peak, corresponding to the silver shell, appeared progressively around 410 nm and became the main component of the absorption band after the fifth addition, turning the suspension color from red to orange. After the sixth addition, the LSPR band became more uniform, displaying a single broad absorbance peak at 430 nm. After the tenth addition, the suspension became milky yellow, due to the scattering properties of these large nanostructures. Dynamic light scattering (DLS) analyses showed an increase of the initial particle hydrodynamic radius from 2 nm to 30 nm for the 1st to the 10th addition respectively, suggesting

an increase of the silver shell thickness from 1 nm to 15 nm (Figure 1B). Finally, a thin gold shell was grown on the silver shell of the Au@Ag^{10}NPs through the sequential addition of citrate and $HAuCl_4$ to Au@Ag^{10}NPs-citrate, leading to Au@Ag^{10}@AuNPs (Scheme 1). The growth of a gold shell in the presence of hydroquinone is known to form urchin-like structures,[31] enhancing the surface area, which could, for instance, augment antibody loading or binding events in potential applications. This additional gold shell drastically changed the optical properties of the NPs, turning the suspension color from yellow to grey (Figure 1C). This observation has already been reported for Au@Ag@Au core-shell-shell nanostructures.[32,33] It is noteworthy that the external gold layer was also added on Au@Ag^{5}NPs-citrate but these particles presented a lower extinction coefficient and a less appealing color as colorimetric reporter compared to Au@Ag^{10}@AuNPs (see Figure S2 for characterizations). Remarkably, the experimental UV-Vis spectra indicated a 3.5-fold increase in molar extinction coefficient for Au@Ag^{5}NPs-citrate and a 9-fold increase for Au@Ag^{10}NPs-citrate, reported as a function of the moles of nanoparticles, compared to the initial AuNPs-citrate (6.10^9 $M^{-1}cm^{-1}$). Predictive extinction coefficients of AuNPs and AgNPs with 37, 49 and 74 nm were compared with the coefficient of our resulting Au@AgNPs in Table S1, confirming the experimental values that were obtained. In contrast to the yellow suspensions of pure 20-50 nm AgNPs, the Au@Ag^{5}NPs-citrate suspensions exhibited an orange color, thanks to the presence of the gold core. As mentioned above, this result is particularly important for designing a colorimetric reporter that can be used in LFAs. It is noteworthy that, when the synthesis of the Au@AgNPs was achieved from 20 nm AuNPs-citrate instead of 37 nm AuNPs-citrate, the absorbance of the silver shell rapidly dominated the LSPR band, resulting in yellow-colored suspensions after only five cycles of additions (Figure S3), providing poor contrast against the membrane. The choice of 37 nm AuNPs as precursor material was furthermore confirmed using predictive UV-Vis spectra of Au@AgNPs, with a final diameter of 50 nm and starting with different Au core sizes (Figure S4). Smaller cores are shown to lead to yellow particles, while larger ones exhibit lower extinction coefficients due to the poorer optical properties of gold.

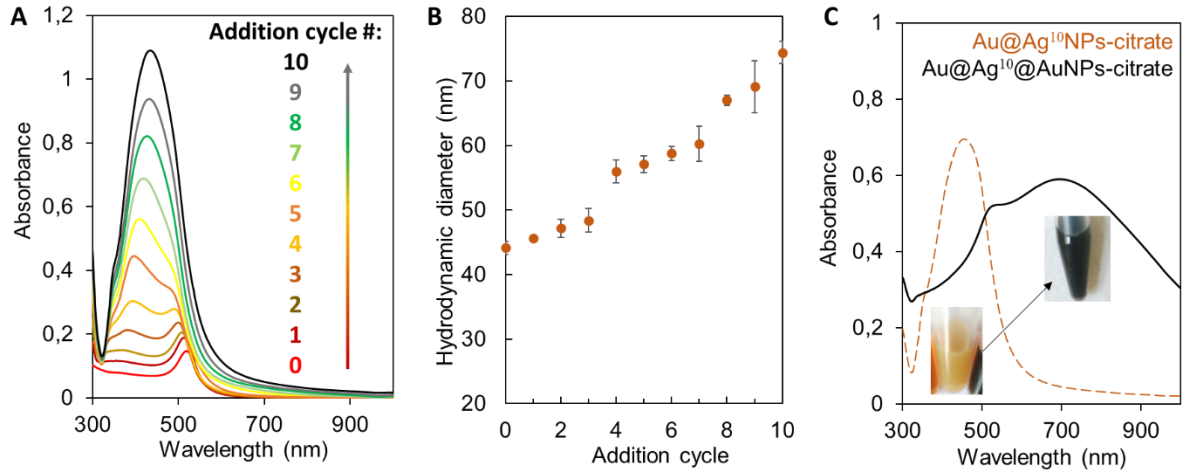

Figure 1: A) UV-Vis spectra monitoring and B) hydrodynamic diameter of core-shell Au@AgNPs-citrate as a function of the number of addition cycles. C) UV-Vis spectra of Au@Ag^{10}NPs-citrate before and after the addition of a final gold shell.

A ligand exchange procedure consisting in the reductive grafting of the calix[4]arene-tetradiazonium salt $X_4(N_2^+)_4$ (see Inset displayed in Scheme 1) was then applied to the three different types of nanoparticles, namely Au@Ag^5, Au@Ag^{10} and Au@Ag^{10}@AuNPs-citrate. To do so, sodium borohydride and $X_4(N_2^+)_4$ were added to the NP suspensions, which were then stirred for 16h. The resulting calixarene-coated nanoparticles, NPs–X_4, underwent three centrifugation cycles to eliminate unbound calix[4]arenes and were subsequently redispersed in water. The size of the NPs–X_4 was determined using Transmission Electron Microscopy (TEM). Au@Ag^{5}NPs-X_4, Au@Ag^{10}NPs-X_4 and Au@Ag^{10}@AuNPs-X_4 exhibited diameters of 49 ± 4 nm, 74 ± 6 nm and 82 ± 10 nm, respectively (Figure 2A-C). It is noteworthy that the size average obtained for the Au@Ag^{10}@AuNPs-X_4 may be less reliable, due to their non-spherical urchin-like structure of the external gold shell (Figure 2C, inset). Analysis of the NPs by dark field microscopy and EDX mapping unequivocally confirmed the core-shell nature of the nanostructures (see Figure 2D for Au@Ag^{10}NPs-X_4, and Figure S5 for Au@Ag^{10}@AuNPs-X_4),[34] indicating the absence of significant galvanic replacement during the synthesis. Furthermore, DLS measurements of the NPs-X_4 were conducted, showing an increase in the hydrodynamic size (ca. 6 nm for both Au@AgNPs-X_4) compatible with the grafting of a monolayer of calixarenes (Figure S6). Confirmation of the presence of the calix[4]arene layer on the nanoparticles surface was achieved through Fourier Transform Infrared Spectroscopy (FTIR). As depicted in Figure 2E, characteristic bands corresponding to the calixarene structure (*i.e.* at *ca.* 3000-2800, 1450 and 1050 cm^{-1} for the CH_2 asymmetric and symmetric stretching,

the aromatic ring stretching and the symmetric COC_{Ar} stretching, respectively) were observed after the functionalization, while bands associated with the citrate ligands were no longer visible (Figure 2E- orange dashed line). FTIR spectra of Au@Ag^{10}NPs-X_4 and Au@Ag^{10}@AuNPs-X_4 are presented in Figure S7A and B, respectively.

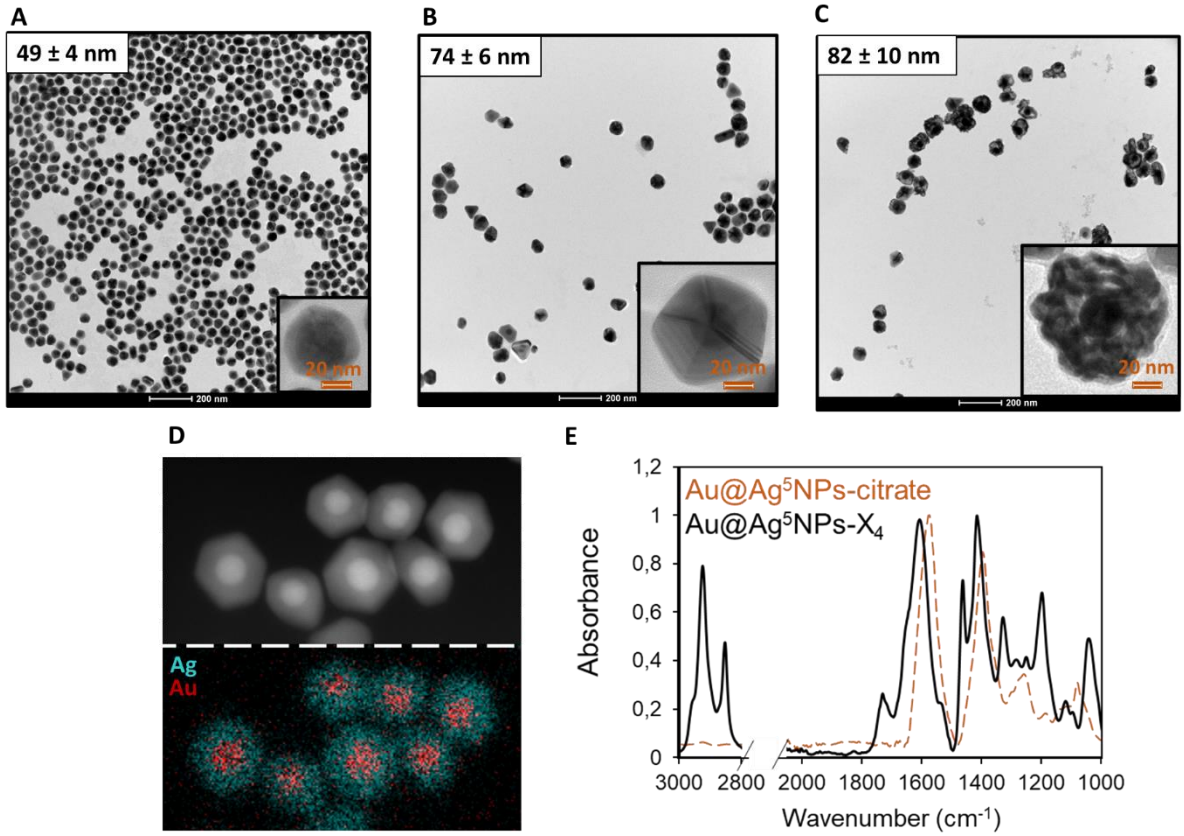

Figure 2: TEM images of A) Au@Ag^{5}NPs-X_4, B) Au@Ag^{10}NPs-X_4, C) Au@Ag^{10}@AuNPs-X_4; D) dark field microscopy and EDX mapping of Au@Ag^{10}NPs-X_4 (blue=Ag; red=Au); E) FTIR spectra of Au@Ag^{5}NPs before and after functionalization with the calix[4]arene.

Stability of calix[4]arenes-coated core-shell nanoparticles. For comparison purposes, the Au@Ag^{5}NPs were also functionalized with a standard thiolated polyethylene glycol derivative, $HS(CH_2CH_2O)_8CH_2CH_2COOH$ (referred to as HS-PEG-COOH), following a standard procedure (see the Experimental Part). The colloidal and chemical stabilities of the Au@Ag^{5}NPs coated by citrate (pristine), calix[4]arene X_4 or HS-PEG-COOH were evaluated using UV-Vis spectroscopy. The suspensions were dispersed in a 1x phosphate buffer saline (PBS) solution, mimicking the ionic strength and pH of body fluids, and UV-Vis spectra were recorded after 2 hours. Most *In-vitro* diagnostic applications necessitate to disperse the particles in PBS, for maintaining the structure of proteins used to functionalize them and maintain their ability to form a complex with their target. Investigating the stability of the NPs in this medium

is therefore crucial. The LSPR band of the Au@Ag^{5}NPs-X$_4$ remained quasi-unaffected in PBS, highlighting the high stability conferred by the calix[4]arene coating (see Figure 3 for the comparison of the three coatings).[35] In contrast, Au@Ag^{5}NPs-citrate instantly aggregated in PBS, as shown by the significant decrease and broadening of the absorption band after only 1 min (Figure 3B). Au@Ag^{5}NPs-S-PEG-COOH exhibited moderate stability, showing a rather pronounced broadening of the LSPR band in the high wavelength region (Figure 3C). Similar high stability in PBS was observed for the Au@Ag^{10}NPs-X$_4$ and Au@Ag^{10}@AuNPs-X$_4$ (Figure S8A and B). The long-term stability of the NPs was also evaluated. The stability of Au@Ag^{5}NPs-S-PEG-COOH and Au@Ag^{5}NPs-X$_4$ were again evaluated in PBS after prolonged storage at room temperature. In contrast to the calixarene-coated Au@Ag^{5}NPs-X$_4$ that maintained colloidal stability over time, the stability of the thiol-coated NPs drastically decreased after one month (Figure S9A and B), in accordance with the lower affinity of thiols for silver surfaces compared to gold surfaces.[36,37] These findings demonstrate that the thin calixarene layer is highly effective in stabilizing the silver surface of the core-shell Au@AgNPs against external stresses, thereby paving the way for their use as colorimetric reporters in LFAs.

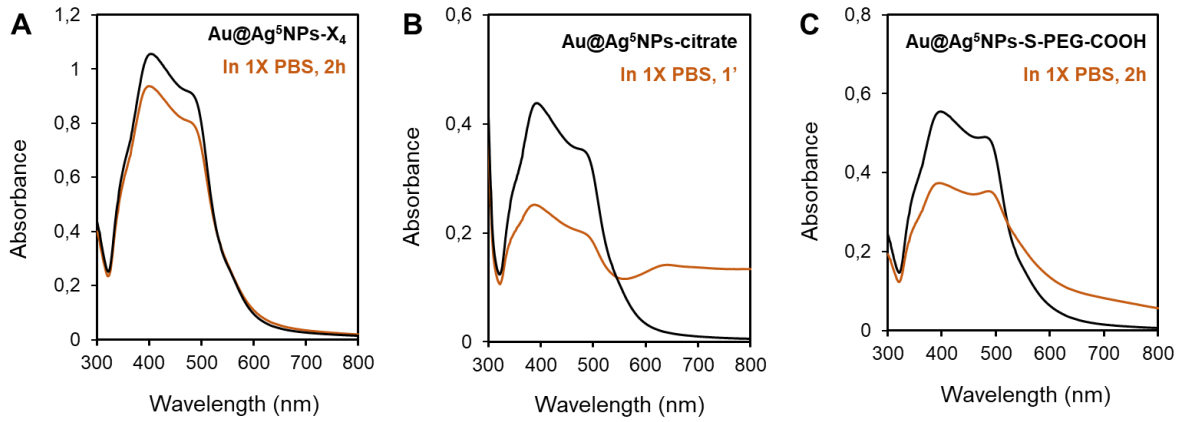

Figure 3: UV-Vis spectra of Au@Ag^{5}NPs stabilized by A) calix[4]arene X$_4$, B) citrate and C) HS-PEG-COOH in water (dark line) or in 1X PBS solution (orange line) after 2 hours.

Au@AgNPs-X$_4$ as colorimetric reporters in lateral flow assays. As mentioned in the introduction, commercial lateral flow assays predominantly rely on the use of gold nanoparticles. Therefore, the starting 37 nm AuNPs-citrate (Scheme 1) were also functionalized with X$_4$(N$_2^+$)$_4$ following the aforementioned procedure (see Figure S10 for the characterization of the resulting AuNPs-X$_4$). These gold nanoparticles were employed as a reference to assess the performance of our core-shell Au@AgNPs-X$_4$. Regarding the LFA, we decided to

investigate the detection of Troponin I, a well-studied cardiac marker.[38] Therefore, the four types of NPs-X_4 (i.e. AuNPs-X_4, Au@Ag^{5or10}NPs-X_4 and Au@Ag^{10}@AuNPs-X_4) were functionalized with an anti-Trop I monoclonal antibody (mAb), produced in mouse, following the standard coupling procedure with EDC and sulfo-NHS. The bioconjugation was conducted at an identical optical density for all batches to ensure a similar total exposed surface area for all candidates. UV-vis spectra of all bioconjugated NPs-X_4 exhibited a sharp and intense LSPR, indicating that no aggregation occurred during the bioconjugation step (Figure S11). To confirm the presence of mAb on the NPs' surface, the nanoparticles were diluted in a running buffer (1% BSA, 0.1% Tween 20 in 1X PBS) at a final optical density (OD) of 0.3, and a strip coated with protein G' at the test line was immersed in the solution. Protein G' has a high affinity for the heavy chain of antibodies and, therefore, the presence of antibodies on the NPs surface leads to their immobilization on the test line, generating a colored signal. To our delight, positive signals were observed for all the functionalized NPs, validating the successful bioconjugation of the antibody (Figure 4A). However, in the case of the Au@Ag^{10}NPs-X_4-mAb, the yellow color of the NPs and their high scattering properties resulted in a faintly visible yellow line, due to a poor contrast with the white membrane (Figure S12). As a result, this type of nanoparticles was omitted from further examination. Given that the nanoparticles used in this study possess very different molar extinction coefficients, quantities of Au@Ag^{5}NPs and Au@Ag^{10}@AuNPs-X_4-mAb approximatively 3.5 times and 9 times lower than that of AuNPs-X_4 were used to generate signals of comparable intensities (Figure 4A). To better compare the potential of the different types of NPs as colorimetric reporters, a similar lateral flow experiment was thus conducted using NPs-X_4-mAb at the same concentration (approximately 20 pM) rather than the same OD. Under these conditions, the test line was much more pronounced for the Au@Ag^{10}@AuNPs-X_4-mAb, whereas the use of the AuNPs-X_4-mAb resulted in a test line that was difficult to discern with the naked eye (Figure 4B). This result aligns with the higher molar extinction coefficient of the core-shell NPs, demonstrating the remarkable potential of these nanomaterials as effective colorimetric reporters.

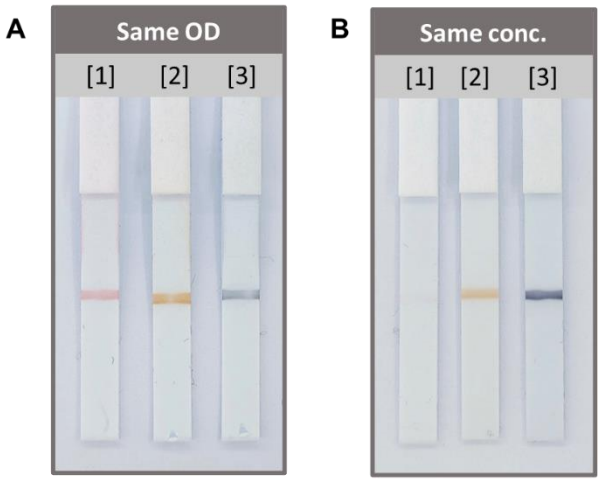

Figure 4: Pictures of Protein G half strip with the different NPs-X_4-mAb A) at the same optical density (OD) and B) at the same concentration.

Finally, the performance of the various types of NPs as colorimetric reporters was evaluated for the detection of Troponin I. For this, the different NPs-X_4-mAb were diluted in a running buffer spiked with different concentrations of Troponin I: 20, 10, 5, 2.5, 1 and 0 ng/mL. After incubating the mixture for 15 minutes, a strip, with a test line composed of a monoclonal antibody recognizing a different Troponin I epitope than the one bound to the NPs, was immersed. Read-out was achieved after 30 minutes, both by naked-eye observation and camera capture. In all cases, an intense signal was observed at the control line (Anti-Mouse Antibody), showing that the experiments proceeded correctly. AuNPs-X_4-mAb presented the weakest signal across the different concentration ranges, and only a very faint signal could be detected at 2.5 ng/mL (Figure 5A). In contrast, the use of Au@Ag^5NPs-X_4-mAb and Au@Ag^{10}@AuNPs-X_4-mAb enabled the detection of Troponin I down to at least 1 ng/mL (Figure 5B and C, respectively). These experiments were conducted in duplicate (Figure S13), and all strips were examined by three distinct observers using naked-eye observation. The best results were obtained with the Au@Ag^{10}@AuNPs-X_4-mAb, as the grey-colored T line generated by these NPs provided a strong contrast to the white membrane, facilitating the detection, particularly at the lowest concentrations. Quantification of the signal intensity was performed using a reported procedure based on ImageJ, and the limit of quantification (LoQ) was determined as 10 times the standard deviation of the background (Figure 5D).[39] The performances of the NPs based on signal intensity ranked as follows: Au@Ag^{10}@AuNPs-X_4 > Au@Ag^5NPs-X_4 > AuNPs-X_4, confirming the naked eye observations. Based on signal

intensity, predictive LoQs of 0.06, 0.35 and 0.9 ng/mL were determined for Au@Ag^{10}@AuNPs-X$_4$, Au@Ag^{5}NPs-X$_4$ and AuNPs-X$_4$, respectively. The core-shell nanoparticles Au@Ag^{10}@AuNPs-X$_4$ emerged as the most promising candidate as a colorimetric reporter for LFA, as they combine strong contrast with the white membrane and the lowest LoQ.

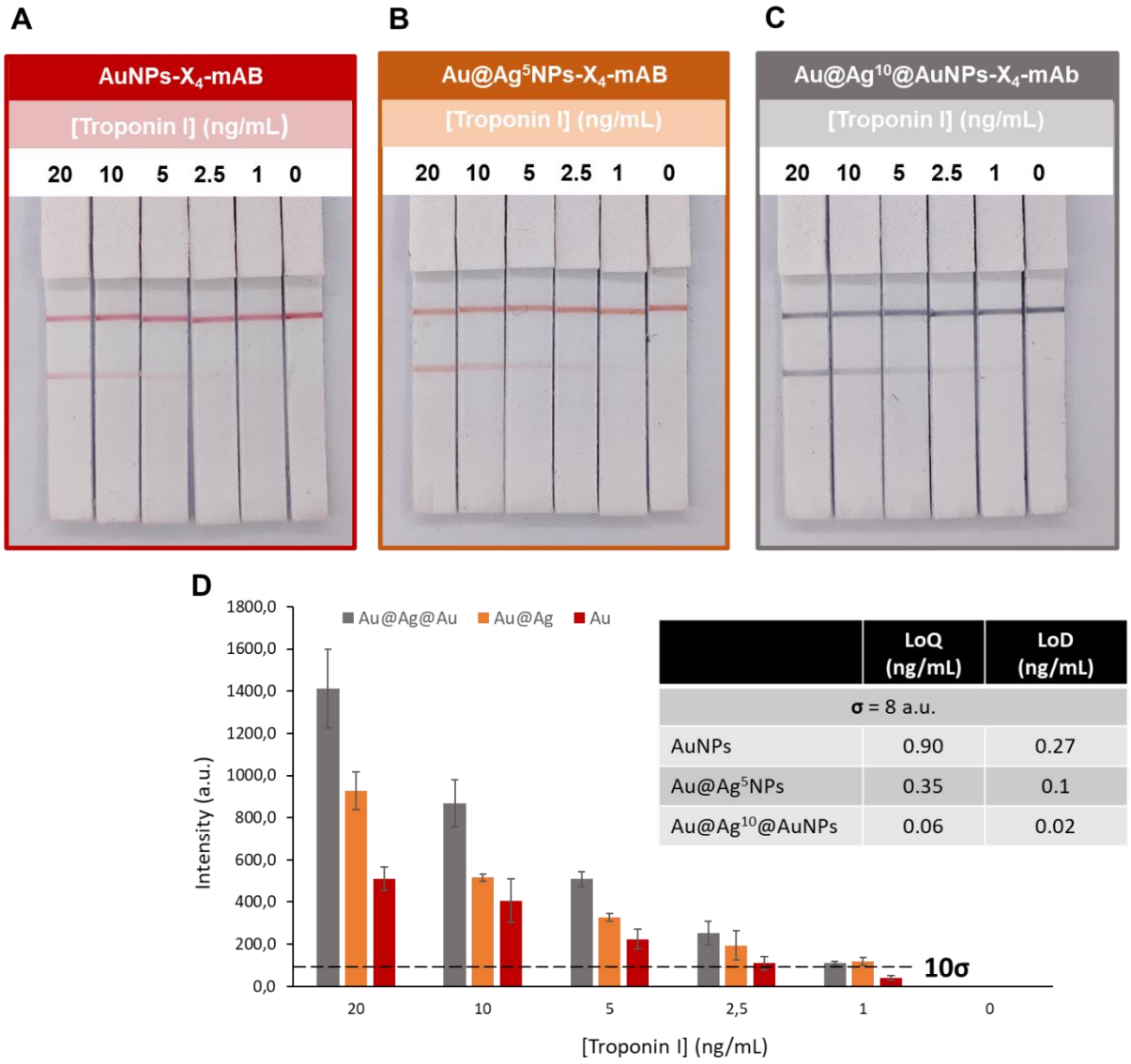

	LoQ (ng/mL)	LoD (ng/mL)
σ = 8 a.u.		
AuNPs	0.90	0.27
Au@Ag^{5}NPs	0.35	0.1
Au@Ag^{10}@AuNPs	0.06	0.02

Figure 5: Pictures of Anti-Troponin I half strip with different concentrations of Troponin I: 20, 10, 5, 2.5, 1, 0 ng/mL using (a) AuNPs-X$_4$-mAb (b) Au@Ag^{5}NPs-X$_4$-mAb (c) Au@Ag^{10}@AuNPs-X$_4$-mAb as colorimetric reporters. (d) Quantification of signal intensity using a reported procedure based on ImageJ software[38] and LoQ calculation. σ corresponding to the standard deviation of background obtained by ImageJ. Experiments were performed in duplicate.

Conclusion

With the aim to develop more efficient colorimetric reporters than classical gold nanoparticles, various types of Au@Ag core-shell nanoparticles were designed. A convenient synthesis method for these core-shell nanoparticles, ensuring strict control over the silver shell thickness, was established. This procedure utilized a seed growth-mediated approach, leveraging the reducing properties of hydroquinone and the stabilizing properties of citrate throughout the colloidal suspension synthesis. Additionally, we examined the impact of an external gold layer on the Au@AgNPs, which significantly altered their optical properties. All core-shell NPs were functionalized with a calix[4]arene layer. The stability of the calixarene-coated Au@AgNPs against external stresses, such as PBS, outperformed that of similar Au@AgNPs functionalized with conventional ligands, such as a thiolated PEG or citrate, particularly for long-term storage. The calixarene coating enabled the covalent bioconjugation of antibodies without inducing noticeable aggregation, which is usually extremely difficult to achieve with NPs exposing an external silver layer, again highlighting its exceptional stability. Compared to 37 nm AuNPs, the core-shell Au@AgNPs exhibited substantially higher molar extinction coefficients. Their performance as colorimetric reporters was subsequently evaluated in a lateral flow assay for the detection of Troponin I. Positive signals were observed down to at least 1 ng/ml with the Au@AgNPs, while the AuNPs exhibited a naked eye limit of detection of 2.5 ng/ml. Furthermore, the grey color of the core-shell Au@Ag^{10}@AuNPs provides a strong contrast against the white NC membrane, facilitating the T line visualization even at low intensities. Remarkably, our assay competes with the limit of quantification of most commercial LFAs for detecting Troponin I. Considering that LFA parameters (buffer, OD of the nanoparticles, antibodies quantities, etc.) were not optimized, this result is particularly promising for the development of highly sensitive assays, expanding the boundaries of LFAs in biomarkers detection. It is important to point out that our initial purpose was to compare the performance of the different colorimetric reporters using the detection of Troponin I as a model system and, therefore, future work will be required to develop a functional assay, especially in body fluid such as plasma. Finally, the different types of core-shell NPs used in this study form a library of colorimetric reporters with distinct optical properties. Compared to the silver nanoplates (AgNPls) we previously reported,[18] this strategy allows to increase significantly the extinction coefficient while maintaining the absorption band in the visible region. Such a library paves the way for the development of multiplexed detection systems capable of targeting multiple proteins simultaneously, thereby enhancing diagnostic reliability. Moreover, as highlighted in

this example, the detection range can be tailored by selecting specific colorimetric reporters based on the relevant LoQ desired for the analyte.

Materials and method

Chemical and Biomolecules. All chemicals were at least of reagent grade. HS-PEG_8-COOH and Protein G' were purchased from Iris Biotech and Sigma Aldrich, respectively. AuNPs-citrate (37 nm) were ordered from NanoFlow. Anti-troponin antibodies, strips and calix[4]arene $X_4(N_2^+)_4$ salt were obtained from X4C.

Characterizations and Measurements. UV−vis absorption spectra were recorded with a UV−vis spectrophotometer in quartz cuvettes. As-synthesized NPs were diluted by a factor of 10 in 1 mL of aqueous solution unless otherwise noted. Attenuated Total Reflection Fourier-Transform Infrared (ATR-FTIR) spectra were recorded at 20 °C on a Shimadzu QATR-S FTIR spectrophotometer. The nanoparticles were centrifugated, and 2 µL of the pellet was deposited on the diamond. Water was removed with a flow of nitrogen gas. Data were processed and analyzed using the instrument software by correcting the baseline, setting apodization at 10 cm^{-1}, and normalizing on the most intense signal. Images of the NPs were obtained with a transmission electron microscope (TEM) equipped with a lanthanum hexaboride (LaB6) crystal at a 200 kV accelerating voltage. The average size and standard deviation were determined by measuring the size of more than 100 NPs for each sample. Samples were characterized by dynamic light scattering (DLS) with back scattering (NIBS 173°) using a Malvern Zetasizer. Measurements were performed at 25 °C and the NPs were dispersed in MilliQ water to obtain 1 mL of NPs (OD = 0.1) in disposable semi-micro cuvettes (PMMA) and multiple DLS measurements were performed. The reported values are the average hydrodynamic diameters obtained from three independent measurements using the Z average as calculated by the Zetasizer software**.** Samples were analyzed in Laboratorio de Microscopias Avanzadas (Zaragoza, ES) for EDS mapping and dark-field imaging using an Analytical Titan.

Core-shell NPs synthesis. ***Au@Ag^{5}NPs.*** In an 8 mL glass vial, 1 mL of AuNPs-citrate 37 nm (OD= 8) was diluted in 4 ml of MilliQ H_2O. Under stirring, 50 µL sodium citrate (15.4 mM), 50 µL hydroquinone (46.4 mM) and 50 µL of $AgNO_3$ (10 mM) were successively added. The additions were repeated 5 times (in total) with a waiting time of 2 minutes between two cycles of additions. ***Au@Ag^{10}NPs.*** In an 8 mL glass vial, 2.5 mL *Au@Ag^{5}NPs* were diluted in 2.5 ml of MilliQ H_2O. Under stirring, 50 µL sodium citrate (15.4 mM) and 50 µL of $AgNO_3$ (10 mM)

were successively added. The additions were repeated 5 times (in total) with a waiting time of 2 minutes between two cycles of additions. ***Au@Ag^{10}@AuNPs.*** In an 8 mL glass vial, 2.5 mL *Au@Ag^{10}NPs* were added. Under stirring, 20 µL sodium citrate (15.4 mM) and 20 µL of $HAuCl_4$ (10 mM) were successively added. The additions were repeated 2 times (in total) with a waiting time of 2 minutes between two cycles of additions.

Calix[4]arene functionalization. In an 8 ml glass vial, 2.5 mL of the appropriate Au@AgNPs were added. Then, 25 µL of $NaBH_4$ (100 mM) and 250 µL $X_4(N_2^+)_4$ (5 mM) were successively added. The mixture was stirred overnight at room temperature**.** The suspension was then transferred in 1.5 mL Eppendorfs and 3 µL of NaOH 1M were added in each Eppendorf. The Eppendorfs were then centrifugated at 2500 g for 15 minutes. The supernatant was discarded, and the particles were resuspended in 5 mM NaOH solution. The cleaning cycle was repeated twice and the particles were ultimately resuspended in MilliQ water.

Thiol functionalization. In a 1.5mL Eppendorf, 1 mL of Au@Ag^{5}NPs was mixed with 10 µL HS-PEG-COOH (0.5 mM) and stirred overnight. The resulting NPs were then centrifugated at 2500 g for 15 minutes. The supernatant was discarded, and the particles were resuspended in a 5 mM NaOH solution. The cleaning cycle was repeated twice, and the particles were ultimately resuspended in MilliQ water.

Bioconjugation of mAb. In a 1.5mL Eppendorf, 150 µL of the appropriate NPs-X_4 were added at an optical density=5. Then, 50 µL MES (100 mM, pH 5.8), 60 µL EDC.HCl (6 mM) and 60 µL Sulfo-NHS (10 mM) were added to the Eppendorf. The activation step was carried out for 1 hour before the tube was filled to 0.75 mL with MilliQ H_2O and centrifuged at 2500 g for 15 minutes at room temperature. The supernatant was discarded, and the pellet was resuspended in 150 µL phosphate buffer (5 mM, pH 8). Then, 10 µL of Anti-troponin I antibody (0.1 mg/mL in 5 mM PB pH 8) were added, and the reaction mixture was stirred for 1 hour at room temperature. Then, 600 µL of a solution of 1% BSA, 0.1% Tween 20 in 5 mM PB pH 8 were added and the centrifuge tube was stirred for 3-5 minutes before being centrifuged for 15 min at 2500 g. Afterwards, the supernatant was discarded, and particles were resuspended in 1 mL of the solution 1% BSA, 0,1% Tween 20 in 5 mM PB pH 8 and once again, centrifuged. After the last cycle, NPs were resuspended in 150 µL of 0.1% Tween 20 in 5 mM phosphate buffer (pH 8). The resulting particles were stored at 4°C.

Assay procedure. In a well of a 96-well plate, 5 µL of the appropriate NPs-X_4-mAb (OD=3) were diluted in 40 µL of running buffer (1% BSA, 0.1% Tween 20 in 1x PBS). Then, 5 µL of

the appropriate stock solutions of Troponin I were added to obtain final concentrations of 20, 10, 5, 2.5, 1 and 0 ng/mL. The mixture was incubated for 15 minutes to allow the formation of the antibody-target complex and then, an anti-Troponin I half strip was immersed in the well. Readout was achieved after 30 minutes and performed with 3 distinct observers. All observed a positive signal down to 2.5 ng/mL for Au NPs-X_4-mAb and 1 ng/mL for Au@Ag^5NPs-X_4-mAb and Au@Ag^{10}@AuNPs-X_4-mAb. Simultaneously, images of the strips were captured by a camera and signal intensities were obtained using a reported procedure using ImageJ.[38]

Supporting information

UV-Vis spectra, TEM, EDX mapping images, DLS, FTIR spectra, predictive UV-Vis spectra of Au@AgNPs, images of half-strip for troponin detection.

ACKNOWLEDGMENTS

This research was supported by the Fonds pour la formation à la Recherche dans l'Industrie et dans l'Agriculture (FRIA-FRS) and the Fonds David et Alice Van Buuren (PhD grant to B.G.). The authors thank the "Fondation Jaumotte-Demoulin" for the acquisition of the equipment necessary for the preparation of the LFA strips.

Conflicts of interest

I. J. is a shareholder of X4C. I. J. and G.B. are consultants for X4C.

References

(1) Borghei, Y.-S.; Hosseinkhani, S.; Ganjali, M. R. "Plasmonic Nanomaterials": An Emerging Avenue in Biomedical and Biomedical Engineering Opportunities. *Journal of Advanced Research* **2022**, *39*, 61–71. https://doi.org/10.1016/j.jare.2021.11.006.

(2) *Nanoparticles: Workhorses of Nanoscience*; De Mello Donegá, C., Ed.; Springer Berlin Heidelberg: Berlin, Heidelberg, 2014. https://doi.org/10.1007/978-3-662-44823-6.

(3) Lenne, Q.; Retout, M.; Gosselin, B.; Bruylants, G.; Jabin, I.; Hamon, J.; Lagrost, C.; Leroux, Y. R. Highly Stable Silver Nanohybrid Electrocatalysts for the Oxygen Reduction Reaction. *Chem. Commun.* **2022**, *58* (20), 3334–3337. https://doi.org/10.1039/D2CC00637E.

(4) Paramelle, D.; Sadovoy, A.; Gorelik, S.; Free, P.; Hobley, J.; Fernig, D. G. A Rapid Method to Estimate the Concentration of Citrate Capped Silver Nanoparticles from UV-Visible Light Spectra. *Analyst* **2014**, *139* (19), 4855. https://doi.org/10.1039/C4AN00978A.

(5) Kelly, K. L.; Coronado, E.; Zhao, L. L.; Schatz, G. C. The Optical Properties of Metal Nanoparticles: The Influence of Size, Shape, and Dielectric Environment. *J. Phys. Chem. B* **2003**, *107* (3), 668–677. https://doi.org/10.1021/jp026731y.

(6) Kong, F.-Y.; Zhang, J.-W.; Li, R.-F.; Wang, Z.-X.; Wang, W.-J.; Wang, W. Unique Roles of Gold Nanoparticles in Drug Delivery, Targeting and Imaging Applications. *Molecules* **2017**, *22* (9), 1445. https://doi.org/10.3390/molecules22091445.
(7) Liu, X.; Atwater, M.; Wang, J.; Huo, Q. Extinction Coefficient of Gold Nanoparticles with Different Sizes and Different Capping Ligands. *Colloids and Surfaces B: Biointerfaces* **2007**, *58* (1), 3–7. https://doi.org/10.1016/j.colsurfb.2006.08.005.
(8) Chen, X.; Ding, L.; Huang, X.; Xiong, Y. Tailoring Noble Metal Nanoparticle Designs to Enable Sensitive Lateral Flow Immunoassay. *Theranostics* **2022**, *12* (2), 574–602. https://doi.org/10.7150/thno.67184.
(9) Deng, Y.; Jiang, H.; Li, X.; Lv, X. Recent Advances in Sensitivity Enhancement for Lateral Flow Assay. *Microchim Acta* **2021**, *188* (11), 379. https://doi.org/10.1007/s00604-021-05037-z.
(10) Mirica, A.-C.; Stan, D.; Chelcea, I.-C.; Mihailescu, C. M.; Ofiteru, A.; Bocancia-Mateescu, L.-A. Latest Trends in Lateral Flow Immunoassay (LFIA) Detection Labels and Conjugation Process. *Front. Bioeng. Biotechnol.* **2022**, *10*, 922772. https://doi.org/10.3389/fbioe.2022.922772.
(11) Mie, G. Beiträge zur Optik trüber Medien, speziell kolloidaler Metallösungen. *Ann. Phys.* **1908**, *330* (3), 377–445. https://doi.org/10.1002/andp.19083300302.
(12) Li, J.; Duan, H.; Xu, P.; Huang, X.; Xiong, Y. Effect of Different-Sized Spherical Gold Nanoparticles Grown Layer by Layer on the Sensitivity of an Immunochromatographic Assay. *RSC Adv.* **2016**, *6* (31), 26178–26185. https://doi.org/10.1039/C6RA03695C.
(13) Medina-Rivera, M.; Cárdenas, W. B.; Erickson, D.; Mehta, S. Gold Nanoshells-Based Lateral Flow Assay for the Detection of Chagas Disease at the Point-of-Care. *The American Journal of Tropical Medicine and Hygiene* **2022**, *107* (2), 323–327. https://doi.org/10.4269/ajtmh.21-1119.
(14) Liu, H.; Dai, E.; Xiao, R.; Zhou, Z.; Zhang, M.; Bai, Z.; Shao, Y.; Qi, K.; Tu, J.; Wang, C.; Wang, S. Development of a SERS-Based Lateral Flow Immunoassay for Rapid and Ultra-Sensitive Detection of Anti-SARS-CoV-2 IgM/IgG in Clinical Samples. *Sensors and Actuators B: Chemical* **2021**, *329*, 129196. https://doi.org/10.1016/j.snb.2020.129196.
(15) Rycenga, M.; Cobley, C. M.; Zeng, J.; Li, W.; Moran, C. H.; Zhang, Q.; Qin, D.; Xia, Y. Controlling the Synthesis and Assembly of Silver Nanostructures for Plasmonic Applications. *Chem. Rev.* **2011**, *111* (6), 3669–3712. https://doi.org/10.1021/cr100275d.
(16) Loiseau, A.; Asila, V.; Boitel-Aullen, G.; Lam, M.; Salmain, M.; Boujday, S. Silver-Based Plasmonic Nanoparticles for and Their Use in Biosensing. *Biosensors* **2019**, *9* (2), 78. https://doi.org/10.3390/bios9020078.
(17) Wang, Y.; Van Asdonk, K.; Zijlstra, P. A Robust and General Approach to Quantitatively Conjugate Enzymes to Plasmonic Nanoparticles. *Langmuir* **2019**, *35* (41), 13356–13363. https://doi.org/10.1021/acs.langmuir.9b01879.
(18) Retout, M.; Gosselin, B.; Adrović, A.; Blond, P.; Jabin, I.; Bruylants, G. Ultra-Stable Silver Nanoplates: Efficient and Versatile Colorimetric Reporters for Dipstick Assays. *Nanoscale* **2023**, *15* (28), 11981–11989. https://doi.org/10.1039/D3NR02378H.
(19) Retout, M.; Jabin, I.; Bruylants, G. Synthesis of Ultrastable and Bioconjugable Ag, Au, and Bimetallic Ag_Au Nanoparticles Coated with Calix[4]Arenes. *ACS Omega* **2021**, *6* (30), 19675–19684. https://doi.org/10.1021/acsomega.1c02327.
(20) Mattiuzzi, A.; Jabin, I.; Mangeney, C.; Roux, C.; Reinaud, O.; Santos, L.; Bergamini, J.-F.; Hapiot, P.; Lagrost, C. Electrografting of Calix[4]Arenediazonium Salts to Form Versatile Robust Platforms for Spatially Controlled Surface Functionalization. *Nat Commun* **2012**, *3* (1), 1130. https://doi.org/10.1038/ncomms2121.

(21) Troian-Gautier, L.; Mattiuzzi, A.; Reinaud, O.; Lagrost, C.; Jabin, I. Use of Calixarenes Bearing Diazonium Groups for the Development of Robust Monolayers with Unique Tailored Properties. *Org. Biomol. Chem.* **2020**, *18* (19), 3624–3637. https://doi.org/10.1039/D0OB00070A.
(22) Troian-Gautier, L.; Valkenier, H.; Mattiuzzi, A.; Jabin, I.; Den Brande, N. V.; Mele, B. V.; Hubert, J.; Reniers, F.; Bruylants, G.; Lagrost, C.; Leroux, Y. Extremely Robust and Post-Functionalizable Gold Nanoparticles Coated with Calix[4]Arenes via Metal–Carbon Bonds. *Chem. Commun.* **2016**, *52* (69), 10493–10496. https://doi.org/10.1039/C6CC04534K.
(23) Retout, M.; Gosselin, B.; Mattiuzzi, A.; Ternad, I.; Jabin, I.; Bruylants, G. Peptide-Conjugated Silver Nanoparticles for the Colorimetric Detection of the Oncoprotein Mdm2 in Human Serum. *ChemPlusChem* **2022**, *87* (4). https://doi.org/10.1002/cplu.202100450.
(24) Gosselin, B.; Retout, M.; Dutour, R.; Troian-Gautier, L.; Bevernaegie, R.; Herens, S.; Lefèvre, P.; Denis, O.; Bruylants, G.; Jabin, I. Ultrastable Silver Nanoparticles for Rapid Serology Detection of Anti-SARS-CoV-2 Immunoglobulins G. *Anal. Chem.* **2022**, *94* (20), 7383–7390. https://doi.org/10.1021/acs.analchem.2c00870.
(25) Bai, T.; Wang, M.; Cao, M.; Zhang, J.; Zhang, K.; Zhou, P.; Liu, Z.; Liu, Y.; Guo, Z.; Lu, X. Functionalized Au@Ag-Au Nanoparticles as an Optical and SERS Dual Probe for Lateral Flow Sensing. *Anal Bioanal Chem* **2018**, *410* (9), 2291–2303. https://doi.org/10.1007/s00216-018-0850-z.
(26) Bi, L.; Dong, J.; Xie, W.; Lu, W.; Tong, W.; Tao, L.; Qian, W. Bimetallic Gold–Silver Nanoplate Array as a Highly Active SERS Substrate for Detection of Streptavidin/Biotin Assemblies. *Analytica Chimica Acta* **2013**, *805*, 95–100. https://doi.org/10.1016/j.aca.2013.10.045.
(27) Zhao, T.; Liang, P.; Ren, J.; Zhu, J.; Yang, X.; Bian, H.; Li, J.; Cui, X.; Fu, C.; Xing, J.; Wen, C.; Zeng, J. Gold-Silver Alloy Hollow Nanoshells-Based Lateral Flow Immunoassay for Colorimetric, Photothermal, and SERS Tri-Mode Detection of SARS-CoV-2 Neutralizing Antibody. *Analytica Chimica Acta* **2023**, *1255*, 341102. https://doi.org/10.1016/j.aca.2023.341102.
(28) Tong, L.; Li, D.; Huang, M.; Huang, L.; Wang, J. Gold–Silver Alloy Nanoparticle-Incorporated Pitaya-Type Silica Nanohybrids for Sensitive Competitive Lateral Flow Immunoassay. *Anal. Chem.* **2023**, *95* (47), 17318–17327. https://doi.org/10.1021/acs.analchem.3c03569.
(29) Liao, J.-Y.; Li, H. Lateral Flow Immunodipstick for Visual Detection of Aflatoxin B1 in Food Using Immuno-Nanoparticles Composed of a Silver Core and a Gold Shell. *Microchim Acta* **2010**, *171* (3–4), 289–295. https://doi.org/10.1007/s00604-010-0431-0.
(30) Bastús, N. G.; Comenge, J.; Puntes, V. Kinetically Controlled Seeded Growth Synthesis of Citrate-Stabilized Gold Nanoparticles of up to 200 Nm: Size Focusing versus Ostwald Ripening. *Langmuir* **2011**, *27* (17), 11098–11105. https://doi.org/10.1021/la201938u.
(31) Dikkumbura, A. S.; Hamal, P.; Chen, M.; Babayode, D. A.; Ranasinghe, J. C.; Lopata, K.; Haber, L. H. Growth Dynamics of Colloidal Silver–Gold Core–Shell Nanoparticles Studied by *In Situ* Second Harmonic Generation and Extinction Spectroscopy. *J. Phys. Chem. C* **2021**, *125* (46), 25615–25623. https://doi.org/10.1021/acs.jpcc.1c06094.
(32) Knauer, A.; Thete, A.; Li, S.; Romanus, H.; Csáki, A.; Fritzsche, W.; Köhler, J. M. Au/Ag/Au Double Shell Nanoparticles with Narrow Size Distribution Obtained by Continuous Micro Segmented Flow Synthesis. *Chemical Engineering Journal* **2011**, *166* (3), 1164–1169. https://doi.org/10.1016/j.cej.2010.12.028.
(33) Karam, T. E.; Smith, H. T.; Haber, L. H. Enhanced Photothermal Effects and Excited-State Dynamics of Plasmonic Size-Controlled Gold–Silver–Gold Core–Shell–Shell

Nanoparticles. *J. Phys. Chem. C* **2015**, *119* (32), 18573–18580. https://doi.org/10.1021/acs.jpcc.5b05110.

(34) EDX mapping measurements were conducted with the aim of confirming the formation of a core-shell structure rather than an alloyed structure. Considering that Au@Ag^{5}NP serves as the precursor to Au@Ag^{10}NP, we deemed the characterization of Au@Ag^{10}NP to be the most pertinent.

(35) The slight decrease in absorbance observed in the case of Au@Ag5NPs-X4 stems from the sticking of the NPs onto the wall of the plastic cuvette utilized for measuring the absorption spectrum in PBS over time. Importantly, it is distinct from the aggregation or the dissolution observed for the NPs stabilized by citrate or thiolated PEG for which the decrease in absorbance is much more important and a broadening of the peak is observed.

(36) *CRC Handbook of Chemistry and Physics: A Ready-Reference Book of Chemical and Physical Data*, 104nd edition, 2023–2024.; Rumble, J. R., Brunno, T. J., Doa, M. J., Eds.; CRC Press: Boca Raton London New York, 2023.

(37) Longo, A.; Carotenuto, G.; Palomba, M.; Nicola, S. D. Dependence of Optical and Microstructure Properties of Thiol-Capped Silver Nanoparticles Embedded in Polymeric Matrix. *Polymers* **2011**, *3* (4), 1794–1804. https://doi.org/10.3390/polym3041794.

(38) Dasgupta, A.; Wahed, A. Cardiac Markers. In *Clinical Chemistry, Immunology and Laboratory Quality Control*; Elsevier, 2014; pp 127–144. https://doi.org/10.1016/B978-0-12-407821-5.00008-5.

(39) Parolo, C.; Sena-Torralba, A.; Bergua, J. F.; Calucho, E.; Fuentes-Chust, C.; Hu, L.; Rivas, L.; Álvarez-Diduk, R.; Nguyen, E. P.; Cinti, S.; Quesada-González, D.; Merkoçi, A. Tutorial: Design and Fabrication of Nanoparticle-Based Lateral-Flow Immunoassays. *Nat Protoc* **2020**, *15* (12), 3788–3816. https://doi.org/10.1038/s41596-020-0357-x.